

Fabrication of New 3D Phantom for the measurement of Geometric Distortion in Magnetic Resonance Imaging System

Sadegh Shurche^{1*}, Mohammad Yousefi Sooteh²

1. Department of Physics and Medical Engineering, School of Medicine, Tehran University of Medical Sciences, Tehran, Iran
2. Department of Medical Physics, School of Medicine, Tabriz University of Medical Sciences, Tabriz, Iran

ARTICLE INFO

Article type:
Original Article

Article history:
Received: Oct 16, 2018
Accepted: Dec 18, 2018

Keywords:
MRI
Distortion
Phantom

ABSTRACT

Introduction: Geometric distortion, an important parameter in neurology and oncology. The current study aimed to design and construct a new three-dimensional (3D) phantom using a 3D printer in order to measure geometric distortion and its 3D reproducibility.

Material and Methods: In this study, a new phantom containing 13,824 reference features (control points) was designed with AutoCAD software, fabricated with a 3D printer, and filled with vegetable oil. This phantom was tested on the Siemens 3 Tesla Prisma MRI model using a 64-channel head coil. Six-slice computed tomography (CT) scan images were used as a reference. Moreover, the reference features of MRI images were matched with those of CT scan images using a 3D reference model. The reproducibility of the phantom was investigated on three different days (three different imaging sessions per day).

Results: The obtained 3D results indicated that the non-uniformity of field and nonlinearity of the gradients and imaging reproducibility could lead to geometric distortion. The mean Euclidean distance error for MRI volume was less than 1 mm. The maximum Euclidean error was 1.5 mm. Distortion in the whole volume was pronounced more specifically at the edges of the magnetic field.

Conclusion: The results showed that the amount of distortion in the middle of the field was less than at its sides. This phantom can be used to check the distortion filters on the device. Furthermore, this phantom can be used to study geometric distortion in scenarios that require a small study volume, such as prostate studies.

► Please cite this article as:

Sadegh Sh, Yousefi soothe M. Fabrication of New 3D Phantom for the measurement of Geometric Distortion in Magnetic Resonance Imaging System. Iran J Med Phys 2019; 16: 377-384. 10.22038/ijmp.2018.35346.1442.

Introduction

Geometric distortion is a major shortcoming of magnetic resonance imaging (MRI), which has a significant influence on the accuracy of volumetric measurement as an important parameter in neurology [1, 2] and oncology [3]. Furthermore, the MRI-based treatment planning in radiotherapy requires high accuracy [4]. Geometric distortion occurs due to the non-linearity of the gradients and the insufficient correction of the non-uniformity of the field [5]. Two precautionary requirements must be met in order to provide a detailed geometric distortion map. First, the number of control points (reference features) must be sufficient, and secondly the phantom should be fixed permanently in the device [6]. Geometric distortion is investigated through the squares of two-dimensional (2D) networks [7-10], cylindrical phantoms [11-13], and thin tubes [14]. The main problem in the 2D studies is the limitation to consider the third dimension. As a result, 3D objects should also be used to investigate geometric displacement. Few reports have been made on the geometric distortion of a 3D survey [15]. Breeuwer et al. [16] constructed a 3D spherical phantom with 437 reference points and precision of less than 0.05 mm. Wang et al. [6] designed a cubic phantom made up of

14.28×14.39×9 mm layers. The phantom consisted of 15 layers, each containing 19×19 reference points, with a total of 10,830 reference points. Phantoms constructed in the above-mentioned studies were used to check the accuracy of volumes. The distances between their reference points were more than 10 mm. However, for smaller volume studies, such as prostate studies [17], the distance between reference points should be smaller.

In our previous study, a 2D phantom was constructed in order to examine geometric displacement in two dimensions [18]. However, in the current study, a new phantom was made with a 3D printer containing 13,824 reference points, which could be used to investigate 3D distortion. The main advantage of this phantom was the 2 mm distance between the points of reference. A computed tomography (CT) scan was used as a reference for matching the features in the MRI images. To achieve this, a 3D reference feature model was used. Reproducibility on the phantom was investigated on three different days through three different imaging sessions a day. Finally, the 3D geometric distortion was determined from the field non-uniformity and the nonlinearity of the gradients and reproducibility.

*Corresponding Author: Tel: +98 (021) 66466383; Fax: +98 (021) 88973653; Email: sadegh.shurche@yahoo.com

Materials and Methods

Phantom Design and Construction

A cubic phantom was designed to measure $102 \times 102 \times 102$ mm (Figure 1) using AutoCAD software (version M.49.0.0 AutoCAD 2016). In the next step, a phantom was fabricated by a company (Kian Pars, Tehran, Iran) using a white, non-porous plastic PA2200 material (a fine powder with polyamide base 12; Figure 2). Considering strength and lightness of this material, it was suitable to be used due to its magnetic properties [19]. The phantom was created by a 3D printer (Quantum Generous model, made in Iran).

The intersection of the lines in the phantom was considered as the reference point (Figure 1). The phantom consisted of 24 layers, each with a 24×24 -point reference layer leading to a total of 13,824 reference points. The reference points were in the volume distribution of $2 \times 2 \times 2$ mm in three directions of x, y, z.

The phantom was filled with vegetable oil (sunflower oil). Oil is preferred to water at high field [7] since it can prevent the susceptibility of magnetic properties in the interface of the phantom and air. The phantom fixated inside a leak-tight container. The phantom was filled, it was placed on a shaking plate immediately for 3 min. This could prevent the trapping of air bubbles in the phantom, which would result in susceptibility artifacts.

Phantom Imaging

Computed Tomography Scan Imaging

In order to properly define the location of the control points, the CT scan of the phantom was performed using a Siemens 6 Slice CT scan device. The phantom was placed on the bed and at the center of the CT scan. The

in-plane resolution was 0.5×0.5 mm and the resolution was 1×1 mm outside the plane

Magnetic Resonance Imaging

To achieve reproducibility and positioning accuracy of the phantom, the axis of the phantom was aligned with the B_0 field accompanied by supports. The phantom was placed at the center of the device and the imaging was performed using the Prisma (Siemens) MRI at the national brain mapping laboratory. Table 1 indicates the details of the scanner used in this study. The imager had a 64-channel head coil, and a 3-Tesla field; other parameters are listed in Table 2. One of the major advantages of 3D gradient echo techniques (e.g., 3D FLASH) is the ability to obtain thin and high-resolution sections that can be reformatted in the orthogonal planes without any significant loss of spatial resolution [20]. The 3D FLASH can be employed to provide high resolution, high contrast, thin section, and T1 weighted images of the body [20]. The device's distortion modifier filter was used in the imaging. The mean time of imaging was 30 min per day (the duration of each imaging was 10 min). When using a phantom, it is essential to know about its relaxation sessions. Having phantom matter, T1 is especially important in choosing the pulse sequence parameters. Therefore, the amount of T1 and T2 of the oil in the phantom were measured on the machine using an inversion recovery sequence and a multi-echo sequence, respectively [21]. A mono-exponential fit was used for both data series. T1 and T2 values were 257 milliseconds and 90 msec, respectively. According to the formula of the intensity of the signal in the investigated FLASH images, the oil signals have to be close to zero to create a maximum differential between the oil and the phantom

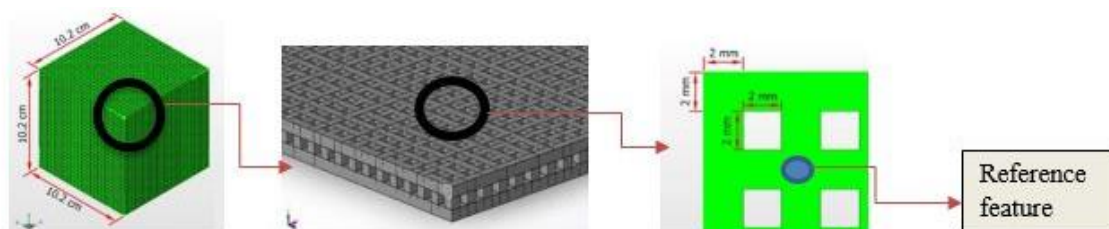


Figure 1. Schematic representation of the phantom used for the study of geometric distortion designed in AutoCAD software (version M.49.0.0 AutoCAD 2016) with the dimensions of $102 \times 102 \times 102$ mm (The intersection of the lines in the phantom is considered a reference point. The phantom consists of 24 layers, each with a 24×24 point reference layer, for a total of 13,824 phantom reference points. The reference points are in volume distribution of $2 \times 2 \times 2$ mm in three directions x, y, z.)

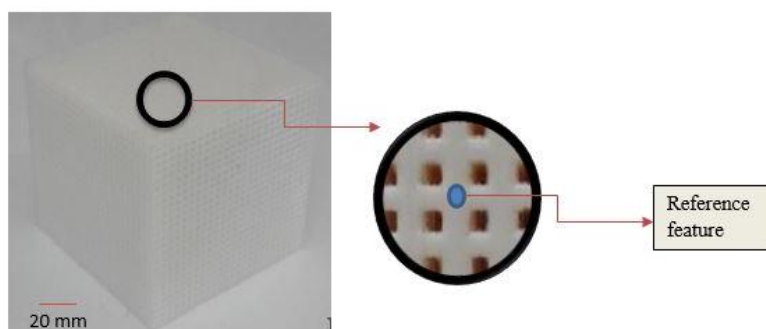


Figure 2. Geometric distortion phantom using a three-dimensional printing method with the dimensions of $102 \times 102 \times 102$ mm and the weight of 1 kg without vegetable oil and 1.250 kg with vegetable oil

Table 1. Details of the scanner in this study using the parameters from the system manual

Vendor	Model	Field(T)	GS (mT/m)	SR(T/m/s)	Homogeneity(ppm)	Diameter(cm)	Length(cm)
Siemens	prisma	3	80	200	1.1 typical1	60	213

1At 24 cm diameter spherical volume (DSV)
(GS: Gradient Strength, SR: Slow Rate)

Table 2. Imaging parameters in this study with the duration of 10 min for each imaging

Sequence	TR/TE (ms/ms)	FA(0)	FOV (mm×mm)	In-plane Resolution(mm×mm)	Slice width(mm)	Receiver Bandwidth (Hz/Pixel)	Number of Excitations
3D FLASH	11/5	30	120×120	0.71×0.71	1	285	1

(FA: Flip Angle, TR: Repetition Time, TE: Echo Time, FOV: Field of View, NEX: Number of Excitations)

Analysis of Images

Detection of Reference Feature

This study relied on the a normalized cross-correlation (NCC) algorithm [27,28] since it is a robust algorithm, which is generally used in image processing [29]. All algorithms used in image analysis were coded using MATLAB software (version 8.3.0.532, Math Works). The image analysis flowchart is shown in Figure 3.

The regulated position of the reference features in a 3D image is g in which $g(x, y, z)$ indicates the intensity value of the image volume of the size $M_x \times M_y \times M_z$ at the points $x, y,$ and $z,$ where, $x \in \{0 \dots M_x - 1\}, y \in \{0 \dots M_y - 1\}, z \in \{0 \dots M_z - 1\}$. A given pattern (p) of the size $N_x \times N_y \times N_z$ is used to represent the pattern. It is possible to use the normalized cross-correlation value (τ) to identify the pattern in image (g) at each point (u, v, w) for g and the pattern p that has been shifted by u steps in the x direction, by v steps in the y direction, and by w steps in the z direction. It is also possible to expand the definition for NCC from 2D to a third dimension express it as:

$$\tau = \frac{\sum_{x,y,z}(g(x,y,z) - \bar{g}_{u,v,w})(p(x-u,y-v,z-w) - \bar{p})}{\sqrt{\sum_{x,y,z}(g(x,y,z) - \bar{g}_{u,v,w})^2 \sum_{x,y,z}(p(x-u,y-v,z-w) - \bar{p})^2}} \quad (1)$$

Where, \bar{p} is the mean value of the pattern (p), $\bar{g}_{u,v,w}$ denotes the mean value of $g(x, y, z)$ within the area of the pattern (p) shifted to (u, v, w) and is calculated by:

$$\bar{g}_{u,v,w} = \frac{1}{N_x N_y N_z} \sum_{x=u}^{u+N_x-1} \sum_{y=v}^{v+N_y-1} \sum_{z=w}^{w+N_z-1} g(x, y, z) \quad (2)$$

The NCC is expensive in terms of computations; however, it is possible to approximate it by applying Fourier-based methods or sum-table techniques [29,30]. In this study, the reference feature (Figure 4) is defined clearly, so the approximation could be used to differentiate it from the background as well as the horizontal and vertical edges. For the approximation, the Fourier-based method was applied in this study [31]. One of the effective functions of CPU is template matching, which estimates matching score images between the template and (color) 2D image and 3D image volume.

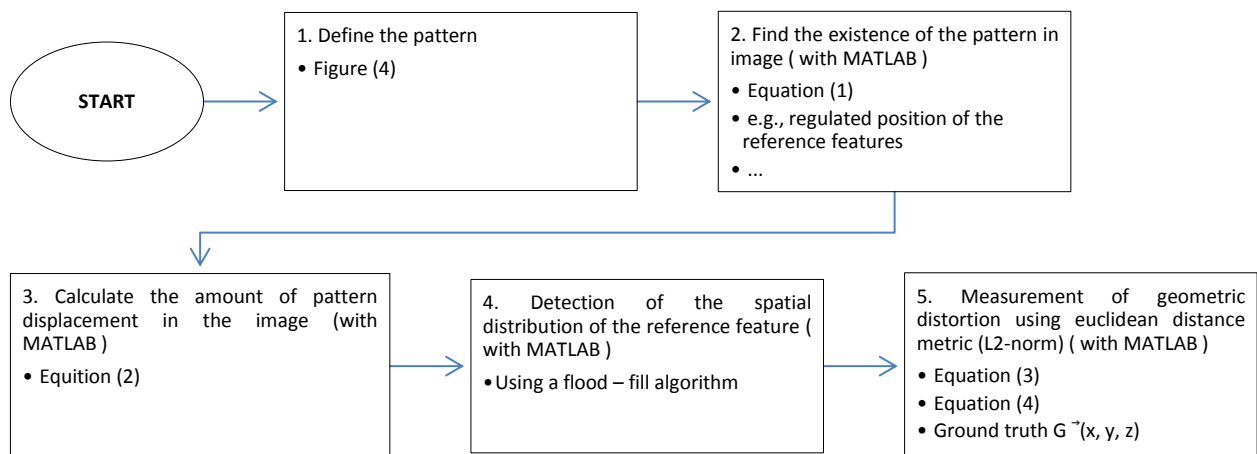


Figure 3. Five steps of image analysis

The CPU calculates:

- The sum of squared difference (SSD; block matching) and robust template matching
- The normalized cross-correlation (NCC), depending on texture rather than illumination

To have template matching, which works robustly with this application, the two images can be merged by the user. The fast Fourier transform-based correlation could be used to apply for the both matching methods. To specify the pattern, the origin of each volume was used, where the central vertex was suitably captured within a pattern of $5 \times 5 \times 5$ voxels from the origin of the CT and MR acquisitions. It is assumed that this point in space has no distortions in the MR acquisition [32] as it is in the magnet isocenter.

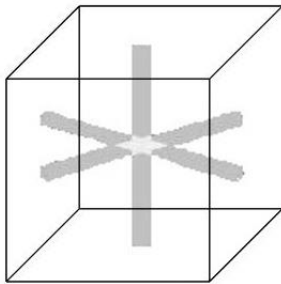


Figure 4. Schematic representation of the reference feature used in the normalized cross-correlation

Detection of the Spatial Distribution of the reference feature

The returning coefficients by the NCC algorithm were set as the volume for every voxel traversed in the NCC algorithm. The NCC coefficients were set as a threshold to have only the maximum correlating points matching the reference feature. Next, a connected-component approach was applied to specify the reference feature. In this regard, a flood-fill algorithm was used to label the connected image pixels [33]. The area connected to a given node in a multi-dimensional array was specified by flood-fill known as seed fill. It is possible to appoint spatial coordinates by finding the centroid of each of the connected pixels through studying the statistics of the connected region, followed by computing a distance transform of the volumetric lattice regarding the isocenter of the volume.

Error Value

To calculate the displacement distance of the reference point, the CT scan image of the phantom was obtained. This value was used as the ground truth $\vec{G}(x, y, z)$ defined in Equation 3. To specify the geometric displacement, Euclidean distance metric (L2-norm) was used. It is shown as the distance between the distances transforms of the ground truth volume and the distance transform of the distorted volume $\vec{C}(x, y, z)$ as defined in Equation 4.

$$\vec{G}(x, y, z) = (x, y, z) \quad (3)$$

$$d(x, y, z) = \|\vec{G}(x, y, z) - \vec{C}(x, y, z)\|_2, (x, y, z) \in B^3 \quad (4)$$

Where, $d(x, y, z)$ shows the Euclidean distance and B^3 shows the set of distances of the reference feature calculated from the isocenter of the CT and MR volumes, respectively, using the distance transform, and $\|\cdot\|_2$ denotes the L2-norm.

Reproducibility Measurement

It was possible to determine the reproducibility measurement of distortion by calculating the mean and standard deviations of the distortion and using Equation [11]:

$$Mean = \sum_{i=1}^n \frac{D_i}{n} \quad (5)$$

$$standard\ deviation = \sqrt{\sum_{i=1}^n \frac{(D_i - Mean)^2}{n-1}} \quad (6)$$

$$CV = \frac{Standard\ deviation}{Mean} \quad (7)$$

Where, D_i is the geometric error in i and n refers to the number of geometric displacement measurement locations.

Imaging was performed 3 sessions in a day without the phantom (CV_1) removal and replacement to confirm the reproducibility of the procedure in the Siemens Scanner. In the next step, the phantom (CV_2) was removed and replaced on 3 different days when the phantom was put through within the brain coil. Based on the expectations, the value of CV_1 would be less than 5% and less than that of CV_2 .

Results

Computed Tomography Scan Imaging

Figure 5 indicates the CT image of the layer, including the reference point. Moreover, the reconstruction of the 3D CT image is shown in Figure 5.

Magnetic Resonance Imaging

The MRI image of the layer between the reference points is indicated in Figure 6. The MRI image of the layer, which includes the reference point is shown in Figure 7. Moreover, the reconstruction of the 3D MRI image is presented in Figure 8. According to the images, there were no susceptibility effects on the images caused by the susceptibility between oil and resin at the bandwidth equal to 285 Hz/pixel.

Geometric Distortion

A 3D image without phantom artifacts was prepared using a CT scan. A 3D image was prepared in MATLAB software (version 8.3.0.532, MathWorks). The control points were compared to the MRI and CT images, and the deviation rate was obtained. Figure 9 illustrates the related Euclidean distance error volumes. The mean Euclidean distance error for MR volume was less than 1 mm.

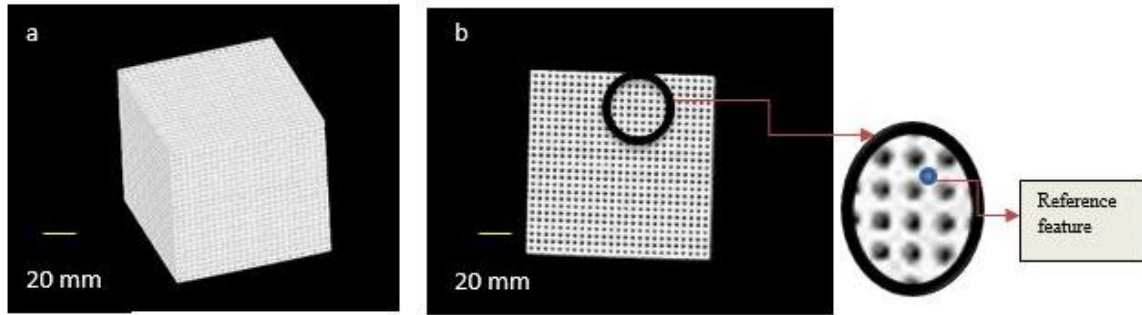


Figure 5. (a) Three-dimensional image reconstructed by a 6-slice Siemens computed tomography scan from a geometric distortion phantom; b) Diagram of an axial cross-sectional image of a phantom (The in-plane resolution was 0.5 x 0.5 mm and the resolution was 1 x 1 mm outside the plane. The reference point is depicted in the image.)

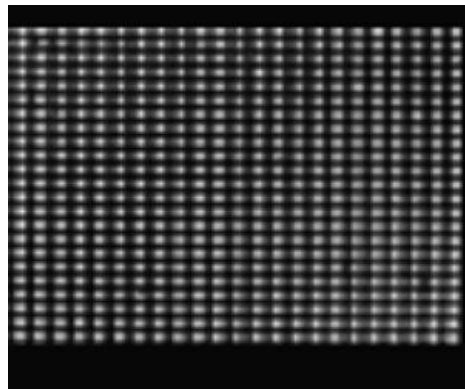


Figure 6. Axial cross-section of the geometric distortion phantom taken from the magnetic resonance imaging device summarized in tables 1 and 2 using the three-dimensional FLASH protocol with parameters TR/TE=11/5 and slice thickness of 1 mm (This image represents the distance between two references features, which itself can be used as a reference feature.)

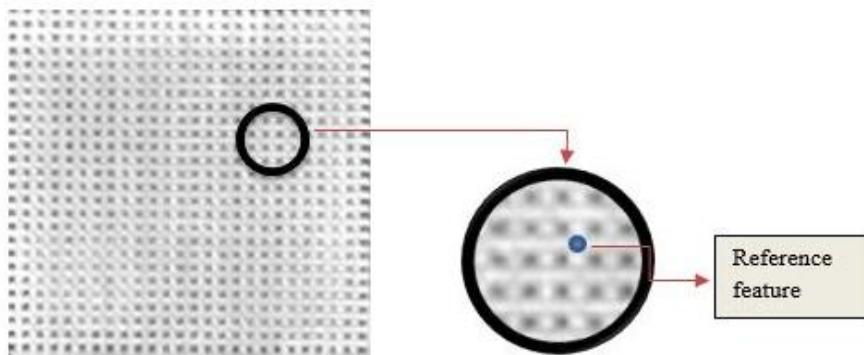


Figure 7. Axial cross section of the geometric distortion phantom taken from the magnetic resonance imaging device summarized in tables 1 and 2 using the three-dimensional FLASH protocol with parameters TR/TE=11/5 and slice thickness of 1 mm. (The reference point is depicted in the image.)

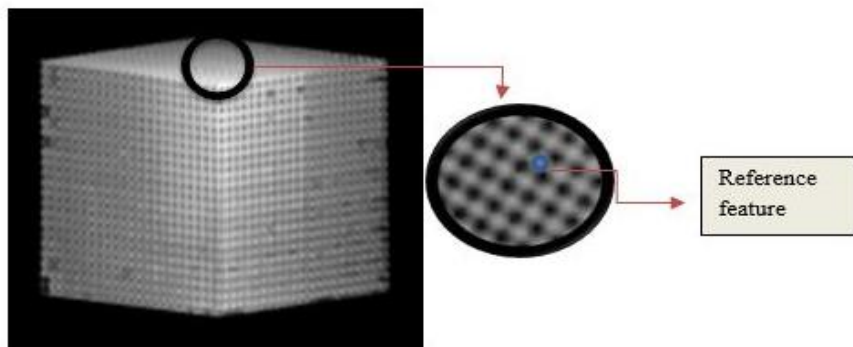


Figure 8. A three-dimensional reconstructed image of the geometric distortion phantom in the MRI device summarized in tables 1 and 2 using the three-dimensional FLASH protocol with parameters TR/TE=11/5 and slice thickness of 1 mm (The reference point is depicted in the image.)

The maximum Euclidean error was 1.5 mm. These results were consistent with the non-homogeneity recognized in a previous study [18] and with the manufacturer’s stated homogeneity as shown in Table 1. The entire volume has distortion, especially at the edges of the magnetic field. Figure 11 shows the geometric distortion in mm for (a) the axial and (b) sagittal control point planes of the phantom for 3 different days.

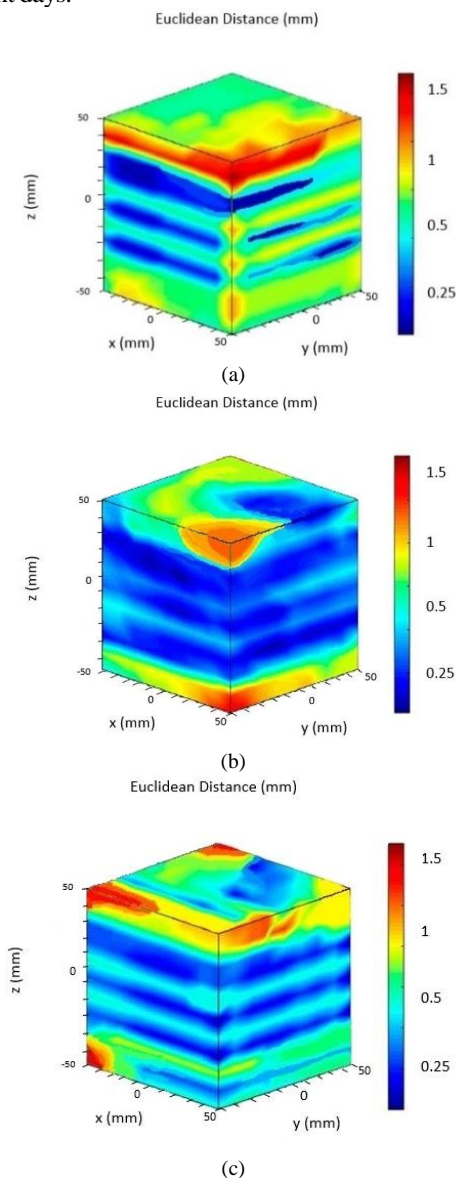


Figure 9. Associated Euclidean distance error volume (a) on the first day, (b) on the second day, and (c) on the third day of measuring reproducibility

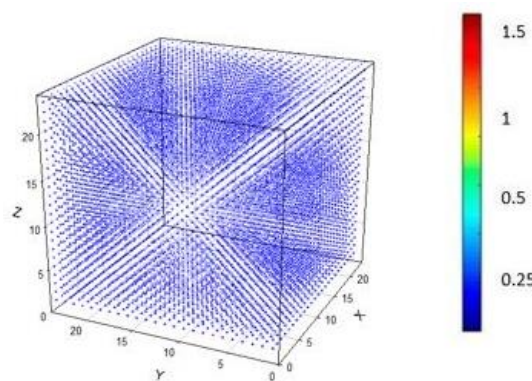


Figure 10. Amount of geometric displacement for the reference point of the phantom (The distortion value increases from the field center to the outside.)

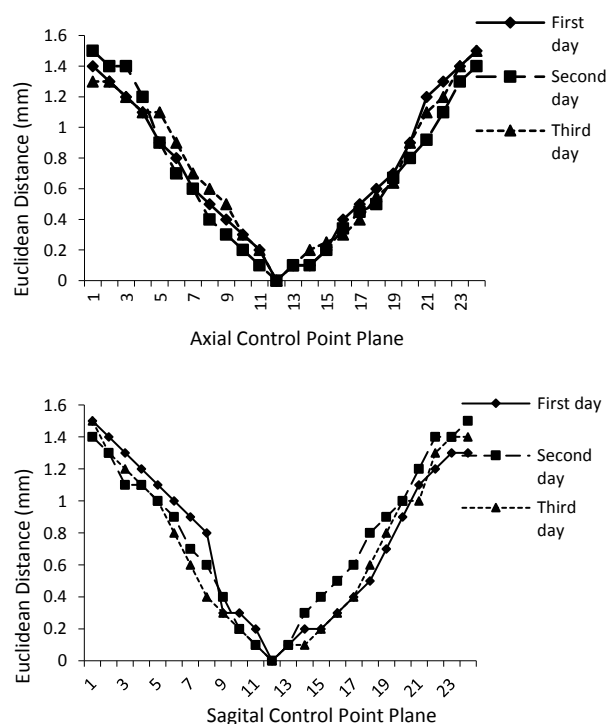


Figure 11. Amount of geometric displacement for (a) the axial and (b) sagittal control point planes of the phantom on three different days (♦ for the first day, ■ for the second day, and ▲ for the third day) (The perpendicular line in each figure represents the central control point plane. In these diagrams, the distortion can be seen from the center of the field to the outside, according to the diagrams, the distortion value increases from the field center to the outside.)

Table 3. Results of measuring the reproducibility of non-uniformity in the device in three directions of x, y, and z, without removing and replacing the phantom (CV₁)

Protocol	Percent of distortion in x axes (mean ±s.d)(1)	Percent of distortion in y axes(mean±s.d)(1)	Percent of distortion in z axes(mean±s.d)(1)
3D FLASH	1.8 ± 0.5	1.7 ± 0.3	1.8 ± 0.2

Table 4. Results of measuring the reproducibility of non-uniformity in the device in three directions of x, y, and z, with removal and replacing the phantom (CV2)

Protocol	Percent of distortion in x axes (mean ±s.d)(2)	Percent of distortion in y axes(mean±s.d)(2)	Percent of distortion in z axes(mean±s.d)(2)
3D FLASH	2 ± 0.2	1.9 ± 0.2	2 ± 0.3

Table 3 and 4 show the results of measuring the reproducibility of non-uniformity in the device in three directions of x, y, and z.

Discussion

In this article, a 3D phantom was fabricated using a 3D printer in order to examine the distortion of an MRI device.

Some studies have shown the image distortion of superconducting magnetic MR systems [26, 34, 35]. Different geometric distortions are also of great importance in Radiation Therapy Treatment Planning

(RTTP). Studies on the issue of reproducibility of image distortion are scarce. [34]. However, the variation of the positional displacements has not been shown officially. Moreover, the image distortion is affected by the bandwidth of the sequences. As a result, a phantom study cannot be conducted through the application of same sequences and the unit planned for use in RTTP. Moreover, the object-related effect that is not similar among patients, remains unexplained.

The designed phantom in the current study outperforms other others available phantoms due to its characteristics. First, in this phantom, there is 2-mm space between the reference points in the x, y, and z pages. However, other studies applied over 2 mm. The mean Euclidean distance error in this study was less than 1.5 mm. Besides, due to the design of the plates, the shape of the phantom was thoroughly appropriate for complete 3D analysis using different coils (body, head, etc.) because it is possible to adjust the number of plates easily. Therefore, it is likely that a single device having a set of different sized plates would fit multiple field of view.

According to Figure 5, the use of non-porous plastic PA2200 material and oil in this phantom is suitable for CT scan imaging, and reference points can be identified on the image. This image could also indicate the accuracy of a 3D printer, which did not result in any phantom making problems.

According to figures 6, 7, and 8, the use of non-porous plastic PA2200 material and oil in this phantom is suitable for MR imaging, and reference points can be identified on the image.

According to Figure 9, the Euclidean distance errors have appeared in the corners of the phantom due to the non-linearity in gradient, non-homogeneity in B1 and B0, or susceptibility of magnetic properties in the interface of phantom and air. To prevent the susceptibility of magnetic properties in the interface of phantom and air, the phantom was fixated inside a leak-tight container. According to our previous studies on this device, these errors may be due to non-homogeneity

in B1 and B0 of MRI [36] or the non-linearity of gradient [18].

Along with other investigations carried out in this line of research, the amount of distortion in the middle of the field was less than its amount at its sides [37]. This is evident in figures 9, 10, and 11.

According to tables 3 and 4, the results of the measurement of the reproducibility of the geometric distortion indicated $CV_1 < CV_2 < 5\%$ as expected.

Another distortion phantom can be investigated through the method introduced in this paper. It is possible to decrease the tolerance and setup time for phantom alignment and template matching by Procrustes methods. The 3D NCC coefficient can also be used for phantoms having 3D patterns with a different center. The coordinates of the control points can be specified through this method concurrently in three directions.

In the next steps, this study aimed to build the phantom with the same distances among control points but with a larger total volume.

Conclusion

This phantom can be used to check the distortion filters on the device.

Volumetric studies in MRI, such as prostate studies, require a high degree of precision. The high accuracy of this phantom makes it qualified to obtain the geometric distortion in such studies.

The method used in this paper is an inexpensive and accurate method for the evaluation of the geometric displacement in the imaging volume.

Acknowledgment

We would like to thank the Food and Drug Administration of the Islamic Republic of Iran and also the National Brain Mapping Lab for their contributions to this project.

References

1. Keller SS, Roberts N. Measurement of brain volume using MRI: software, techniques, choices and prerequisites. *J Anthropol Sci.* 2009;87:127-51.
2. Oghabian MA, Faeghi F, Tohidnia MR. Effect of phase-encoding reduction on geometric distortion and BOLD signal changes in fMRI. *Iranian Journal of Medical Physics.* 2012;9(4):275-81.
3. Harvey H, Orton MR, Morgan VA, Parker C, Dearnaley D, Fisher C, et al. Volumetry of the dominant intraprostatic tumour lesion: intersequence and interobserver differences on multiparametric MRI. *The British journal of radiology.* 2017;90(1071):20160416.

4. Fraass BA, McShan DL, Diaz RF, Ten Haken RK, Aisen A, Gebarski S, et al. Integration of magnetic resonance imaging into radiation therapy treatment planning: I. Technical considerations. *International Journal of Radiation Oncology* Biology* Physics*. 1987;13(12):1897-908.
5. Mallozzi R. *Geometric Distortion in MRI*. The Phantom Laboratory, Inc. 2015.
6. Wang D, Doddrell DM, Cowin G. A novel phantom and method for comprehensive 3-dimensional measurement and correction of geometric distortion in magnetic resonance imaging. *Magnetic resonance imaging*. 2004; 22(4):529-42.
7. Price RR, Axel L, Morgan T, Newman R, Perman W, Schneiders N, et al. Quality assurance methods and phantoms for magnetic resonance imaging: report of AAPM nuclear magnetic resonance Task Group No. 1. *Medical physics*. 1990; 17(2):287-95.
8. Kawanaka A, Takagi M. Estimation of static magnetic field and gradient fields from NMR image. *Journal of Physics E: Scientific Instruments*. 1986 ;19(10):871.
9. Mizowaki T, Nagata Y, Okajima K, Kokubo M, Negoro Y, Araki N, et al. Reproducibility of geometric distortion in magnetic resonance imaging based on phantom studies. *Radiotherapy and Oncology*. 2000; 57(2):237-42.
10. Ashkanmehr M, Riyahi Alam N, Oghabian MA, Ghasemzadeh A, Bakhtiary M, Ghanaati H, et al. Assessment of Reproducibility of Geometric Distortion in MRI using Phantom Measurements. *Iranian Journal of Medical Physics*. 2005; 2(3):1-8.
11. Walton L, Hampshire A, Forster DM, Kemeny AA. A phantom study to assess the accuracy of stereotactic localization, using T1-weighted magnetic resonance imaging with the Leksell stereotactic system. *Neurosurgery*. 1996; 38(1):170-8.
12. Walton L, Hampshire A, Forster DM, Kemeny AA. Stereotactic localization with magnetic resonance imaging: a phantom study to compare the accuracy obtained using two-dimensional and three-dimensional data acquisitions. *Neurosurgery*. 1997;41(1):131-9.
13. Yu C, Apuzzo ML, Zee CS, Petrovich Z. A phantom study of the geometric accuracy of computed tomographic and magnetic resonance imaging stereotactic localization with the Leksell stereotactic system. *Neurosurgery*. 2001;48(5):1092-9.
14. Sumanaweera T, Glover G, Song S, Adler J, Napel S. Quantifying MRI geometric distortion in tissue. *Magnetic resonance in medicine*. 1994 ;31(1):40-7.
15. Baldwin LN, Wachowicz K, Thomas SD, Rivest R, Fallone BG. Characterization, prediction, and correction of geometric distortion in MR images. *Medical physics*. 2007;34(2):388-99.
16. Breeuwer MM, Holden M, Zylka W. Detection and correction of geometric distortion in 3D MR images. In *Medical Imaging 2001: Image Processing*. 2001 ;4322:1110-21.
17. Mazaheri Y, Goldman DA, Di Paolo PL, Akin O, Hricak H. Comparison of prostate volume measured by endorectal coil MRI to prostate specimen volume and mass after radical prostatectomy. *Academic radiology*. 2015;22(5):556-62.
18. Shurche S, Alam NR. Investigating the geometric distortion in 3 tesla MRI images based on the phantom studies. *Frontiers in Biomedical Technologies*. 2017;4(1-2):42-8.
19. Filippou V, Tsoumpas C. Recent advances on the development of phantoms using 3D printing for imaging with CT, MRI, PET, SPECT, and ultrasound. *Medical physics*. 2018 ;45(9):e740-60.
20. Runge VM, Wood ML, Kaufman DM, Nelson KL, Traill MR. FLASH: clinical three-dimensional magnetic resonance imaging. *RadioGraphics*. 1988; 8(5):947-65.
21. Tofts PS, Du Boulay EP. Towards quantitative measurements of relaxation times and other parameters in the brain. *Neuroradiology*. 1990; 32(5):407-15.
22. Buxton RB, Edelman RR, Rosen BR, Wismer GL, Brady TJ. Contrast in rapid MR imaging: T1-and T2-weighted imaging. *J Comput Assist Tomogr*. 1987 ;11(1):7-16.
23. Elster AD. Gradient-echo MR imaging: techniques and acronyms. *Radiology*. 1993;186(1):1-8..
24. Ernst RR, Anderson WA. Application of Fourier transform spectroscopy to magnetic resonance. *Review of Scientific Instruments*. 1966 Jan;37(1):93-102.
25. Haase A, Frahm J, Matthaei D, Hanicke W, Merboldt KD. FLASH imaging. Rapid NMR imaging using low flip-angle pulses. *Journal of Magnetic Resonance (1969)*. 1986 Apr 1;67(2):258-66.
26. Winkler ML, Ortendahl DA, Mills TC, Crooks LE, Sheldon PE, Kaufman L, Kramer DM. Characteristics of partial flip angle and gradient reversal MR imaging. *Radiology*. 1988 Jan;166(1):17-26.
27. Gonzalez R. *RE Woods Digital Image Processing using MATLAB*. 2003;.
28. Jafar M, Jafar Y, Dean C, Miquel M. Assessment of Geometric Distortion in Six Clinical Scanners Using a 3D-Printed Grid Phantom. *Journal of Imaging*. 2017 Sep;3(3):28.
29. Briechle K, Hanebeck UD. Template matching using fast normalized cross correlation. In *Optical Pattern Recognition XII 2001 Mar 20 (Vol. 4387, pp. 95-103)*. International Society for Optics and Photonics.
30. Crow FC. Summed-area tables for texture mapping. In *ACM SIGGRAPH computer graphics 1984*; 18(3): 207-12.
31. kroon DJ. *Fast/Robust Template Matching - File Exchange*. 2009. Available from: <https://uk.mathworks.com/matlabcentral/fileexchange/24925-fast-robust-template-matching?requestedDomain=www.mathworks.com>.
32. Doran SJ, Charles-Edwards L, Reinsberg SA, Leach MO. A complete distortion correction for MR images: I. Gradient warp correction. *Physics in Medicine & Biology*. 2005; 50(7):1343..
33. Vincent L. Morphological Grayscale Reconstruction in Image Analysis: Applications and Efficient Algorithms. *IEEE transactions on image processing*. 1993;2(2):176-201.
34. Fransson A, Andreo P, Pötter R. Aspects of MR image distortions in radiotherapy treatment planning. *Strahlentherapie und Onkologie*. 2001; 177(2):59-73.
35. Walton L, Hampshire A, Vaughan P, Forster DM, Kemeny AA, Radatz MW. Distortion in magnetic resonance images obtained for stereotactic localization. Case report. *Journal of neurosurgery*. 2000;93:191-2.
36. shurche S. Measurement of Radio Frequency Non-Homogeneity in MRI. *Paramedical Sciences and Military Health*. 2018 Mar 1;12(4):62-9..
37. Orth RC, Sinha P, Madsen EL, Madsen EL, Frank G, Frank G, et al. Development of a unique phantom to assess the geometric accuracy of magnetic resonance imaging for stereotactic localization. *Neurosurgery*. 1999 Dec 1;45(6):1423-31.